trimers. This internal consistency is gratifying, and it can be taken as another confirmation that all the patterns have been properly assigned. The difference between the bent/linear trimers and the triangular trimers lies in the J' values, i.e. the Mn^{2+}–Mn^{2+} interactions, which are quite significant in the triangular case but rather unimportant for the other trimers. This is, of course, expected since nearest-neighbor Mn^{2+}–Mn^{2+} contacts only occur in the triangle. And the parameter value of $2J' = -2.0$ cm^{-1} found in our analysis is close to the corresponding value $2J = -1.4$ cm^{-1} found for nearest-neighbor Mn^{2+}–Mn^{2+} dimers in the similar lattice $CdCl_2$.[17]

6. Conclusions

We have been able to directly observe and measure the regular energy splitting pattern that results from exchange interactions in trimers like Mn^{2+}–Ti^{2+}–Mn^{2+}. Besides the regular energy intervals, the spin-level structure is characterized by its *apparent ferromagnetic* ordering of the levels. This does not mean, however, that there are any truly ferromagnetic interactions in the cluster. Both J and J' are antiferromagnetic. The level ordering is a result of the dominance of the Ti^{2+}–Mn^{2+} interactions J compared to the Mn^{2+}–Mn^{2+} interactions J'. In a classical picture the most stable configuration thus corresponds to a parallel alignment of the two Mn^{2+} moments. The apparent ferromagnetic ordering of energy levels follows from the fact that the Mn^{2+} magnetic moments ($S_{Mn} = {}^5/_2$) are larger than the Ti^{2+} ($S_{Ti} = 1$) magnetic moment.

Due to its *high selectivity* as well as *sensitivity* the spectroscopic technique is superior to bulk techniques for the determination of such cluster properties. Deviations from the regular splitting pattern are readily observed, and thus the weaker effects like biquadratic exchange and Mn^{2+}–Mn^{2+} interactions become directly accessible to experiment. Site-selective spectroscopy allows the determination of individual cluster properties in the same crystal and thus a comparison under well-defined conditions.

Acknowledgment. We are grateful to Christian Reber for many useful discussions. This work was financially supported by the Swiss National Science Foundation.

Appendix

With the coupling scheme

$$\mathbf{S}' = \mathbf{S}_{Mn1} + \mathbf{S}_{Mn2}$$
$$\mathbf{S} = \mathbf{S}' + \mathbf{S}_{Ti} \qquad \text{(A1)} = \text{(8)}$$

we use the functions $|(S_{Mn1}\, S_{Mn2})\, S'\, S_{Ti}\, S\rangle$ or, abbreviated $|S'\, S\rangle$, as our basis for the energy calculation. The matrix of the operator

$$\hat{H}_{Trimer} = -2J(\mathbf{S}_{Ti}\cdot\mathbf{S}_{Mn1} + \mathbf{S}_{Ti}\cdot\mathbf{S}_{Mn2}) - 2J'(\mathbf{S}_{Mn1}\cdot\mathbf{S}_{Mn2}) - j[(\mathbf{S}_{Ti}\cdot\mathbf{S}_{Mn1})^2 + (\mathbf{S}_{Ti}\cdot\mathbf{S}_{Mn2})^2] \quad \text{(A2)} = \text{(5)}$$

is not diagonal in this basis. Off-diagonal elements arise from the biquadratic term between functions $|S'\, S\rangle$ and $|S'\, -2\, S\rangle$. Energy differences between these states are large (cf. Figure 2), and we can neglect the off-diagonal elements. Considering only diagonal elements, we can derive the eigenvalues of the three terms in eq A2 separately:

$$E(S',S) = -J[S(S+1) - S'(S'+1) - 2] - J'[S'(S'+1) - {}^{35}/_2] + j\cdot X \qquad \text{(A3)}$$

To evaluate $j\cdot X$ we use the procedure of ref 11. Inclusion of the biquadratic exchange parameter j also leads to a correction of the bilinear term:

$$j\cdot X = \frac{j}{4}[S(S+1) - S'(S'+1) - 2] + E_{biq}(S',S) \quad \text{(A4)}$$

The remaining biquadratic term $E_{biq}(S',S)$ can be expressed as[11]

$$E_{biq}(S',S) = 2[a_2(\mathrm{Ti,Mn})]M_{TiMn}(S',S) \qquad \text{(A5)}$$

with the matrix element

$$M_{TiMn}(S',S) = (-1)^S(2S+1)\begin{Bmatrix} S' & S' & 2 \\ {}^5/_2 & {}^5/_2 & {}^5/_2 \end{Bmatrix}\begin{Bmatrix} S' & S' & 2 \\ 1 & 1 & S \end{Bmatrix} \qquad \text{(A6)} = \text{(7)}$$

where the material in braces represents $6-j$ symbols, and the coefficient is

$$a_2(\mathrm{Ti,Mn}) = -\frac{1}{6}j[(2S_{Ti}-1)(2S_{Ti}+3)(2S_{Mn}-1)(2S_{Mn}+3)(S_{Ti}+1)(2S_{Ti}+1)(S_{Mn}+1)(2S_{Mn}+1)S_{Ti}S_{Mn}]^{1/2} \quad \text{(A7)}$$

Inserting $S_{Ti} = 1$ and $S_{Mn} = {}^5/_2$ we get

$$a_2(\mathrm{Ti,Mn}) = -10(14^{1/2})j \qquad \text{(A8)}$$

Combining eq A3–A8, we get the final expression:

$$E(S',S) = \left(-J + \frac{j}{4}\right)[S(S+1) - S'(S'+1) - 2] - J'[S'(S'+1) - {}^{35}/_2] - 20(14^{1/2})jM_{TiMn}(S',S) \quad \text{(A9)} = \text{(6)}$$

with $M_{TiMn}(S',S)$ as given in eq A6.

Registry No. Ti^{2+}, 15969-58-1; Mn^{2+}, 16397-91-4; $MgCl_2$, 7786-30-3.

(17) McCarthy, P. J.; Güdel, H. U. *Inorg. Chem.* **1986**, *25*, 838.

Contribution from the Department of Chemistry and Materials Science Center, Cornell University, Ithaca, New York 14853-1301

Deformations in Mixed-Valence Cu(I)–Cu(II) Polymers

Paul Sherwood and Roald Hoffmann*

Received April 14, 1988

Some remarkable $Cu_2X_2^-$ (X = Br, Cl) chains recently synthesized by Willett are the impetus to this work. These present one-dimensional extended arrays with well-defined localized perturbations from a basic edge-sharing tetrahedral geometry. We address the electronic structure of these mixed-valence Cu(I)–Cu(II) systems by a construction that begins from a $CuCl_4^{2-}$ ion of S_4 symmetry, progressing through a $Cu_2Cl_6^{3-}$ dimer to the $Cu_2Cl_4^-$ polymers. The energy changes that result from various symmetry-lowering twists and bond length deformations are small, but they are understandable in terms of an orbital overlap and symmetry analysis. Our calculations suggest that the polymer ground states are likely to be magnetic insulating ones and their structures strongly influenced by crystal-packing factors.

Quasi-one-dimensional materials have had a special place in experimental and theoretical solid-state chemistry for many years.[1] While they provide simple models of use in the teaching and understanding of solid-state electronic structure, their low di-

0020-1669/89/1328-0509$01.50/0

mensionality confers upon them a susceptibility to structural distortions and electronic instabilities not found in materials of more isotropic structure.

In the structures of inorganic, transition-metal-containing, one-dimensional materials it is often possible to recognize coordination polyhedra familiar from molecular transition-metal chemistry. The chain structures are built up by the sharing of ligands. The multitude of resulting structures include octahedra, sharing vertices, edges, and faces,[2a-g] trigonal prisms and square antiprisms sharing faces, and tetrahedra,[2h,i] sharing vertices or edges.[3] This paper is concerned with the electronic structure of two novel members of this last class.

Willett has recently reported[4] the isolation and characterization of $[NEt_4][Cu_2Cl_4]$, as a byproduct of the crystal growth of $[NEt_4]_4[Cu_4Cl_{12}]$. The structure is best described as a chain of $CuCl_4$ tetrahedra sharing edges, with a repeat unit of four copper atoms, and is shown in **1**. The one-dimensional chains run along

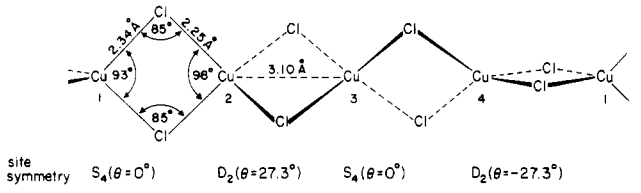

1

the crystallographic *c* axis of the tetragonal crystal. They are effectively isolated from each other by the tetraethylammonium ions; the distance between the crystallographic 2-fold axes on which the chains lie is 7.9 Å.

In this remarkable polymer there are two inequivalent copper sites, differing in both the Cu–Cl bond lengths and the coordination geometry. Half of the copper atoms sit on sites of S_4 symmetry, while the others, with shorter Cu–Cl bond lengths, have local D_2 symmetry. There is a single negative charge on the Cu_2Cl_4 unit, so we are led to a mixed-valence 1:1 Cu(I)–Cu(II) system. The presence of two distinct Cu environments suggests that we should adopt a localized description in which the Cu(II) atoms are assigned to the D_2 sites, class II in the classification[5] of Robin and Day. The local geometry at the D_2 sites is close to the Jahn–Teller-distorted "flattened tetrahedral" D_{2d} geometry expected for the $CuCl_4^{2-}$ ion,[6,7] as are the bond lengths. The distortion of the intervening Cu(I) centers from T_d to S_4 results in a Cu–Cu separation of 3.10 Å, indicative of little direct metal–metal bonding.

The geometrical feature that we will concentrate on in this study is the twisting distortion which relates this structure, **1**, to one with S_4 symmetry at every center. We measure this twist at a given metal atom by the angle θ, which is the deviation from 90° of the angle between the two $CuCl_2$ planes, as shown in **2**. The

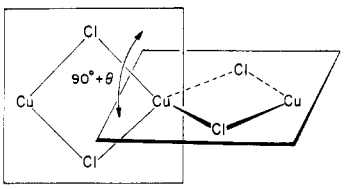

2

fact that these twist angles are equal and opposite for Cu(2) and Cu(4) in **4** gives the structure its repeat unit of four copper atoms.

Since the report of the structure of **1**, Willett has prepared and characterized by X-ray crystallography another mixed-valence Cu(I)–Cu(II) chain.[8] The complex structure contains a $[Cu_2Br_4^-]_\infty$ chain, cocrystallized with 3,5-dibromo-2,6-diaminopyridinium and $CuBr_4^{3-}$ ions, giving an overall stoichiometry of $[C_5H_2Br_2(NH_2)_2N]_4Cu_3Br_8\cdot 2H_2O$.

The geometry of the repeat unit of the chain, which contains two Cu atoms, is shown in **3**. As in **1**, this appears to be a

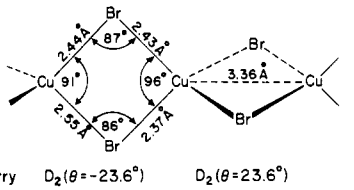

3

localized mixed-valence compound, but in this case the localization is not revealed in the dihedral twist distortions, which are the same at all centers, but in the bond lengths and angles alone. The crystallographic symmetry of this system is much lower than in **1**, as can be seen from the bond lengths in **3**. In particular, there is no crystallographic 2-fold axis along the chain direction, and the two Cu(1)–Br bond lengths differ by 0.11 Å (the crystallographic esd on these quantities is 0.01 Å). It may be that further refinement of this structure, and characterization of further examples, will show this to be a typical distortion of chains of this type. For the present, however, we have chosen to study model complexes idealized to D_2 symmetry at each site.

We wish to understand the localization and deformation processes in these unique mixed-valence polymers. The reader is unlikely to have missed some conceptual connections to the fascinating, developing story of the high-T_c superconductors of the $YBa_2Cu_3O_7$ type: copper, copper chains, mixed valence. It is true that the coordination environment, the dimensionality, and the nature of the mixed valence (there apparently Cu(II)–Cu(III)) are different in the two systems. Still, the analogies bear thinking about.

At first glance, there are two obvious approaches to the study of the electronic structure and geometry of these copper halide complexes. On one hand, we could ignore the fact that the copper centers are coupled together and consider the Jahn–Teller distortions expected from a localized valence model. On the other hand, we could consider the chain as a one-dimensional system; we might then look for ways in which the distortions allow the mixing of filled and unfilled crystal orbitals, as in the Peierls distortions,[9] and thus lower the total energy of the system. We

(1) For articles on the physical and electronic properties of one-dimensional materials see for example: (a) *Crystal Chemistry and Properties of Material with Quasi-One-Dimensional Structures*; Rouxel, J., Ed.; D. Reidel: Dortrecht, Dordrecht, The Netherlands, 1986. (b) Synthesis and Properties of Low-Dimensional Materials; Miller, J. S., Epstein, A. J., Eds. *Ann. N.Y. Acad. Sci.* **1978**, *313*.

(2) For some leading references see the experimental references in these theoretical papers: (a) Whangbo, M.-H.; Schneemeyer, L. F. *Inorg. Chem.* **1986**, *25*, 2424. (b) Whangbo, M.-H.; Canadell, E.; Schlenker, C. *J. Am. Chem. Soc.* **1987**, *109*, 6308. (c) Whangbo, M.-H.; Foshee, M. J.; Hoffmann, R. *Inorg. Chem.* **1980**, *19*, 1723. (d) Hughbanks, T.; Hoffmann, R. *J. Am. Chem. Soc.* **1983**, *105*, 1150. (e) Wijeyesekera, S. D.; Hoffmann, R. *Inorg. Chem.* **1983**, *22*, 3287. (f) Burdett, J. K.; Hughbanks, T. *Inorg. Chem.* **1985**, *24*, 1741. (g) Shaik, S.; Bar, R. *Inorg. Chem.* **1983**, *22*, 735. (h) Hoffmann, R.; Shaik, S.; Scott, J. C.; Whangbo, M.-H. *J. Solid State Chem.* **1980**, *34*, 263. (i) Whangbo, M.-H.; Gressier, P. *Inorg. Chem.* **1984**, *23*, 1228.

(3) Silvestre, J.; Hoffmann, R. *Inorg. Chem.* **1985**, *24*, 4108 and references therein.

(4) Willett, R. D. *Inorg. Chem.* **1987**, *26*, 3423.

(5) Robin, M. B.; Day, P. *Adv. Inorg. Chem. Radiochem.* **1967**, *10*, 248.

(6) Structural studies and reviews: (a) Smith, D. W. *Coord. Chem. Rev.* **1976**, *21*, 93. (b) *Molecular Structure by Diffraction Methods*; Specialist Periodical Reports; The Chemical Society: London, 1973; Vol. 1, p 642.

(7) Theoretical studies: (a) Lohr, L. L., Jr.; Lipscomb, W. N. *Inorg. Chem.* **1963**, *2*, 911. (b) Ballhausen, C. J.; Bjerrum, N.; Dingle, R.; Eriks, K.; Hare, C. R. *Inorg. Chem.* **1965**, *4*, 514. (c) Demuynck, J.; Veillard, A.; Wahlgren, U. *J. Am. Chem. Soc.* **1973**, *95*, 5563. (d) Elian, M.; Hoffmann, R. *Inorg. Chem.* **1975**, *14*, 1058. (e) Burdett, J. K. *J. Chem. Soc., Faraday Trans. 2* **1974**, *70*, 1599.

(8) Willett, R. D. Personal communication.

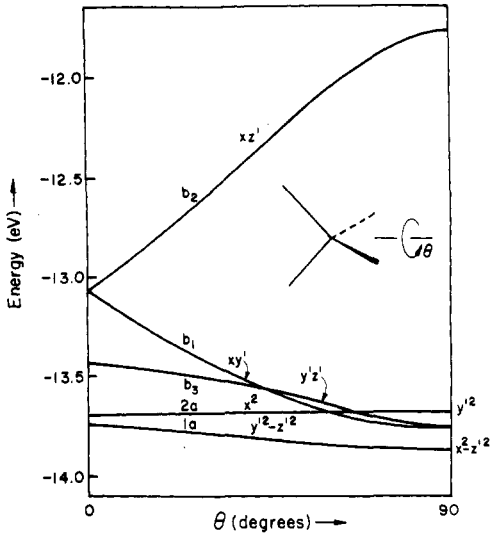

Figure 1. Energies of the d orbitals of $CuCl_4$ as a function of the twist angle, θ. The dominant character of the orbitals at an intermediate angle of twist is given. Note that there is much mixing in the a orbitals, so that the orbital composition evolves with θ as indicated.

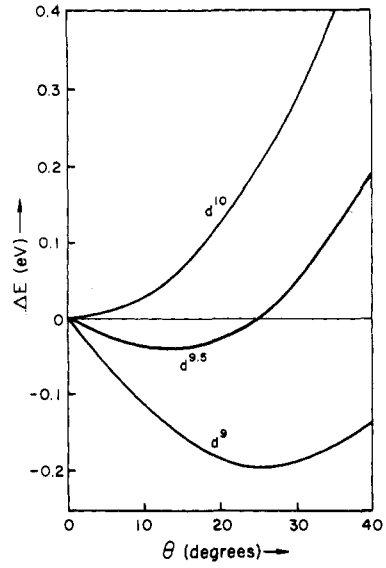

Figure 2. Change in total energies of the ions $CuCl_4^{n-}$ (n = 3, d^{10}; n = 2, d^9) as a function of twist angle θ. Also shown is the $d^{9.5}$ curve.

would then see whether the localization of valence suggested by the crystallographic results can be explained as a consequence of this mixing. In this paper, we will try to combine these two approaches; we will build up the band structure from monomer and dimer units, which have been extensively studied, and at each stage in this construction consider the energetics of the twisting distortion **2** at each center.

Construction of the Chains: The Monomer

In this section we will consider how the band structures of the one-dimensional copper halide chains can be derived from the molecular orbitals of the constituent $CuCl_4$ "monomers". In particular we will be interested in the tendency for an idealized structure (which has $\theta = 0°$ and all bond lengths equal) to undergo twisting distortions of the types observed in **1** and **3**, and we will discuss the way in which the conformational preferences of the $CuCl_4$ units are affected by the coupling together of these units to form an infinite chain.

The energies of the five d orbitals of the $CuCl_4$ molecule as a function of the "twist" distortion θ are shown in Figure 1. At $\theta = 0°$ the molecule has S_4 symmetry with a smaller Cl–Cu–Cl angle of 95.3°. This geometry has been chosen to be consistent with the Cu···Cu nonbonding separation of 3.10 Å and mean Cu–Cl separation of 2.30 Å observed in **1**. The calculations throughout this paper are of the extended Hückel type, with details provided in the Appendix.

At $\theta = 0°$, the energy level diagram differs most from the two below three pattern expected for a tetrahedral ion in the splitting of the t_2 block, into e (xz and xy) and a (yz) levels. We have chosen a coordinate system in which the x axis will become the propagation axis of the chain, and the halide ligands of the undistorted (S_4) structure lie in the xz and xy planes.

For $\theta > 0°$, the twisting of one Cl–Cu–Cl plane lowers the symmetry to D_2 and breaks the degeneracy of the high-lying e set. The four halide ligands approach coplanarity as $\theta \rightarrow 90°$, and in this rectangular-planar (D_{2h}) geometry the energetically higher of these two d orbitals lies in the xz plane.

The three t_2-derived orbitals in the D_2 complex are symmetry distinct, but the two highest, b_1 and b_2, are mixtures of xz and xy in the coordinate system we have used to describe the molecular geometry. Since these two orbitals are responsible for driving all of the structural distortions we will discuss in this paper, we have chosen to define an alternative "local"[10] coordinate system (x, y', z') as shown in **4**, and the orbitals in Figure 1 are labeled according

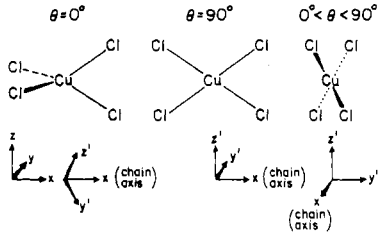

4

to this scheme. The x axis remains unchanged, but y' and z' are chosen to be parallel to the two other C_2 axes in the molecule. The basis vectors for this coordinate system are defined by the relations

$$y' = y \sin(\theta/2 + 45°) - z \cos(\theta/2 + 45°)$$

$$z' = y \cos(\theta/2 + 45°) + z \sin(\theta/2 + 45°)$$

so that the two coordinate systems coincide when $\theta = 90°$. We will find that, in the oligomeric complexes (even when the point group symmetry at Cu is actually lower than D_2), the d orbitals which are antisymmetric with respect to the 2-fold axis along the x axis can be most conveniently described in terms of their xy' and xz' character when the ligand field splitting effects predominate.

For d^9 Cu(II) the total energy of the d electrons is lowest in the rectangular-planar geometry. The extent of the observed distortion will depend on the degree to which these ligand field effects are opposed by interligand repulsions and loss of metal–ligand bonding through the Cu 4p orbitals.[7] Figure 2 shows the variation in total energy as a function of the twist angle θ, for d counts of 9 (Cu(II)), 9.5, and 10 (Cu(I)).

The twisted geometry is clearly energetically favored for the d^9 count, and this preference is classified as a first-order Jahn–Teller distortion, as it involves the loss of orbital degeneracy. Structural studies of the $CuCl_4^{2-}$ ion have shown a range of geometries between tetrahedral and square planar,[6] but in most cases the deformation is probably best described by a D_{2d} distortion coordinate, rather than the twist distortion considered here. In the context of the complexes discussed here, this "flattening"

(9) (a) Peierls, R. E. *Quantum Theory of Solids*; Oxford University Press: London, 1955; p 108. (b) Burdett, J. K. *Prog. Solid State Chem.* **1984**, *15*, 173. (c) Whangbo, M.-H. In ref 1a.

(10) We describe this choice of coordinate system as local to reflect the fact that in an oligomeric or polymeric complex the relative orientations of these axes for the different copper atoms need not be the same; we will use a different local coordinate scheme for each center.

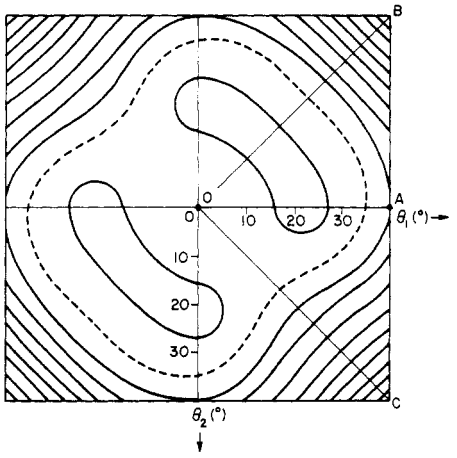

Figure 3. Contour plot showing the change in total energy of the dimer $Cu_2Cl_6^{3-}$ as a function of the two independent twist angles θ_1 and θ_2. The zero contour is shown by a dashed line. Contours are shown at intervals of 0.05 eV; those contours lying inside the zero-energy contour correspond to negative relative energies.

distortion along the x axis would lead to unacceptably close Cu–Cu contacts. However, it is more important in systems where the d counts are lower and metal–metal bonding is significant, such as the related $[FeS_2^-]_\infty$ chains.[3]

In Figure 2 we have shown how the total energy varies with θ for a 9.5-electron count. Since this curve could also be thought of as an average of d^9 and d^{10} curves, it will be instructive when we come to consider the mixed-valence oligomers where distortion simultaneously occurs at both formal Cu(I) and Cu(II) centers.

The $Cu_2Cl_6^{3-}$ Dimer

The next stage in our construction of the polymers is the fusion of two $CuCl_4$ units to form the dimer Cu_2Cl_6. As we have noted, **1** and **2** are class II mixed-valence complexes with adjacent Cu(I) and Cu(II) sites, and we will choose to consider the $Cu_2Cl_6^{3-}$ dimer, with a total of 19 d electrons, as a model for part of these chains.

The construction of dibridged dimers from tetrahedral and square-planar monomer units has already been described in some detail,[11] and only a brief description of the higher lying orbitals (derived from monomer xy and xz) is needed here. These orbitals for a dimer constructed from two monomers of S_4 symmetry, are shown in **5**. In the absence of any interaction we would expect

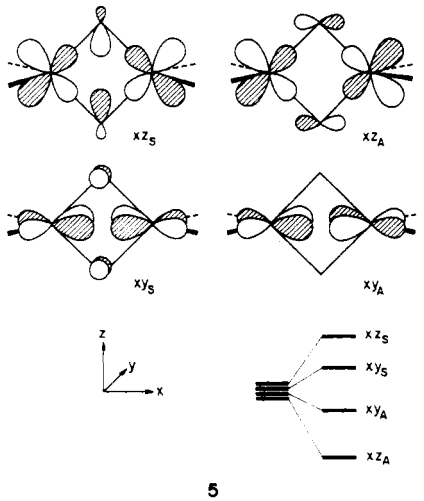

5

four degenerate levels. However, the symmetric and antisymmetric combinations of the xy and xz orbitals are split in energy, as a result of their differing overlap with the orbitals of the bridging ligands. This splitting is largest for the xz pair, since these lie in the plane of the bridging ligands and have the strongest antibonding overlap with Cl s, x, and z orbitals. The factors that determine whether the symmetric or antisymmetric combination has the largest overlap have been discussed before in the context of the superexchange interaction in the d^9–d^9 dimer $Cu_2Cl_6^{2-}$.[12] In general, the symmetric functions show a larger ligand overlap if the Cu–Cl–Cu angle is less than 90° or if the contribution of the ligand s functions is important. The xy_S and xy_A orbitals are split in the same way, since the xy_S combination has an interaction with the π-donor bridging ligand that is totally absent in the antisymmetric function. The smaller splitting reflects the smaller overlaps; these xy orbitals interact more strongly with the terminal ligands rather than the bridges. In $Cu_2Cl_6^{3-}$, which has 19 metal valence electrons, there is only one hole in this system; i.e., the highest xz_S orbital is half-filled.

We will now consider the energetics of the twist distortion for $Cu_2Cl_6^{3-}$. We allow independent distortion at each Cu center and describe the distorted geometry by the two parameters θ_1 and θ_2 as shown in **6**. $\theta_1 = \theta_2 = 0°$ corresponds to the D_{2h} structure (with

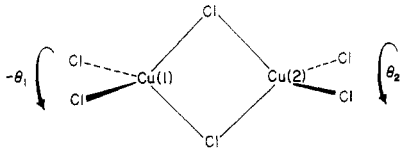

6

approximate local S_4 symmetry at each center) and $\theta_1 = -90°$, $\theta_2 = 90°$ to the planar structure. Figure 3 is a potential energy surface constructed from extended Hückel calculations at various values of θ_1 and θ_2. It is instructive to consider the form we would expect for this surface if the total energy change associated with a distortion could be obtained by adding together the contributions from two monomer units with the same geometries as the two copper centers in the dimer. In this case the contribution for one center would follow the d^9 curve and the other would follow the d^{10} curve. The lowest total energy would occur when one center retained its undistorted S_4 local geometry and would have a total energy minimum at 0.2 eV below the undistorted geometry when the other center had a twist angle of about 25°. Geometries in which both centers were distorted equally ($\theta_1 = -\theta_2$ and $\theta_1 = \theta_2$) would have considerably higher energies. They would vary with θ in the same way as the curve labeled $d^{9.5}$ in Figure 2 but would have twice the magnitude. The maximum stabilization would be 0.1 eV. As the total energies for $\theta_1 = -\theta_2$ and $\theta_1 = \theta_2$ would be equal, the contour plot would have 4-fold symmetry.

Examination of Figure 3 shows the extent to which interaction between the two centers, via the bridging ligands, alters the situation. The minima expected around $\theta_1 = 0°$, $\theta_2 = 25°$, and equivalent points appear, but they are very shallow (a stabilization of only 0.06 eV). These minima are connected by a shallow trough (θ_1 negative, θ_2 positive). This suggests that from this simple picture, which does not include relaxation effects, the localized valence structures (in which one center, associated with a d^{10} count, remains undistorted) are not going to be strongly preferred over delocalized structures in which both copper atoms are equivalent. We also observe that the plot does not have 4-fold symmetry, the energy corresponding to $\theta_1 = -\theta_2$ being a little lower than that corresponding to $\theta_1 = \theta_2$.

The origin of these differences lies, of course, in the "through-bond" or, rather, "through-ligand" interaction between xy and xz orbitals on the two centers. We are interested in the stabilizing or destabilizing effects of that interaction on the equilibrium twisting angle. Even though these orbitals are destabilized by local ligand field effects (mixing with Cl donor orbitals), the twisting deformation is driven by a stabilization arising from the e set (please refer to Figure 1) being split and

(11) Summerville, R. H.; Hoffmann, R. *J. Am. Chem. Soc.* **1976**, *98*, 7240.

(12) Hay, P. J.; Thibeault, J. C.; Hoffmann, R. *J. Am. Chem. Soc.* **1975**, *97*, 4884.

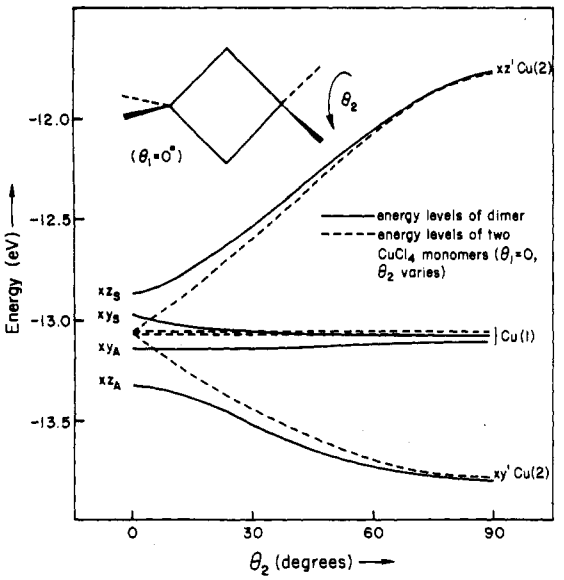

Figure 4. Selected d orbital energies of the $Cu_2Cl_6^{3-}$ dimer as a function of the twist angle θ_2 when $\theta_1 = 0°$. The dashed lines indicate the corresponding d orbital energies of two $CuCl_4$ monomers with the same twist angles.

occupied by 3.5 electrons (for $d^{9.5}$). In the dimer there is a further stabilization, operating near $\theta = 0°$, arising from the through-ligand interaction. Since this is a crucial point, let us explore it in some more detail.

We can see from **5** that the splitting of the four important d levels in $Cu_2Cl_6^{3-}$ occurs more or less symmetrically about the level of the e eset in the S_4 monomer. As there are nine d electrons occupying these four orbitals, the splitting can be viewed as a net stabilization for these electrons as a result of the coupling of the two centers. If the magnitude of this "stabilization" were constant as a function of the angles θ_1 and θ_2, and if we assume that this interaction is the only important change that occurs when we move from the monomer to the dimer, we might expect the total energy of the dimer to behave in a similar way on distortion to the sum of monomer energies. In Figure 4 we have plotted the orbital energies for the case where $\theta_1 = 0°$, corresponding to the direction 0A in Figure 3. As the distortion proceeds, the orbital energies become progressively closer to the levels expected for a pair of monomers with the same coordination environments, which are shown in Figure 4 by the dotted lines. The highest and lowest orbitals become localized on Cu(2), the distorted Cu. In the figure they are labeled according to their predominant contributions, as xz' and xy' (where we are using a local coordinate system for Cu(2) as described above for $CuCl_4$). The monomer levels become an increasingly better model as the orbitals become more localized, because there is then no symmetry restriction on the overlap that these orbitals have with the bridging ligands. As a result the stabilization of the nine d electrons referred to above for $\theta = 0°$ is lost as the distortion proceeds. The depth of the energy minimum is reduced.

Another way of viewing this effect is to note that the energy splitting at $\theta_1 = \theta_2 = 0°$ breaks the 2-fold degeneracy present in the monomers. Consequently, the first-order Jahn-Teller effect is now absent, and all the orbital energies have a zero derivative with respect to our distortion coordinate. These levels must mix for a net stabilization to take place.

A similar effect occurs in the case of the symmetric distortion in which $\theta_1 = -\theta_2$, along the line OB in Figure 3. Again there is no first-order contribution to the energy change. However, this distortion retains a mirror plane perpendicularly bisecting the Cu–Cu vector and the molecular orbitals will be symmetric and antisymmetric combinations of the metal d functions at all geometries. A considerable splitting between these combinations persists in the distorted geometries, and the changes induced in the energies of distortion by the interligand coupling are not as great as in the asymmetric distortion. The line OC in Figure 3 also represents a deformation in which both centers are distorted, but in this case the molecular mirror plane is lost. Consequently, the "through-ligand" coupling of the corresponding d orbitals on the two centers is also lost, and the total energy is a little higher at a point on this line than the corresponding point on the line OB.

One-Dimensional $CuCl_2$ Chains

We are now in a position to consider the band structures of the polymeric materials. As in the dimers, the tendency of these structures to undergo distortions will be set by the orbitals at the top of the d band. This is a result of the high d-electron count. A previous discussion[3] of topologically similar tetrahedral chain compounds, including $[FeS_2^-]_\infty$, has focused on the pairing and folding distortions that result from lower d-electron counts, d^5–d^7.

The model structure we will use for the undistorted chain is shown in **7**. We have chosen the unit cell to contain one of the

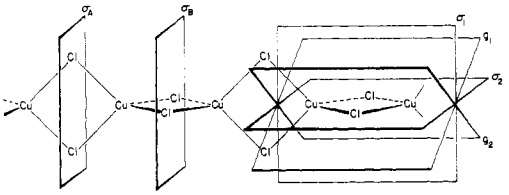

7

dimer units of the above discussion. Also shown in this diagram are some of the symmetry elements that will be useful in classifying the crystal orbitals. σ_A, σ_B, σ_1, and σ_2 are mirror planes; g_1 and g_2 are glide planes coupling reflection with a half-cell translation.

The construction of the crystal orbitals that arise from xy and xz is straightforward at the two high-symmetry points in the Brillouin zone, Γ ($k = 0$) and X ($k = \pi/a$). At Γ, a good approximation for these four crystal orbitals may be obtained by the addition of translational symmetry to the dimer orbitals of **5**. xy_S and xz_S will both give rise to crystal orbitals that are symmetric with respect to σ_A of **7**. As a result of the translational symmetry present at Γ, these two orbitals will be symmetric with respect to σ_B as well. They are clearly equivalent, degenerate orbitals, interconverted by the glide planes g_1 and g_2. We shall label them 2E. Similarly xy_A and xz_A give rise to a pair of degenerate crystal orbitals (1E), which are antisymmetric with respect to both σ_A and σ_B. Representative orbitals are shown in **8**. By direct analogy with the dimer splitting pattern **5**, we would

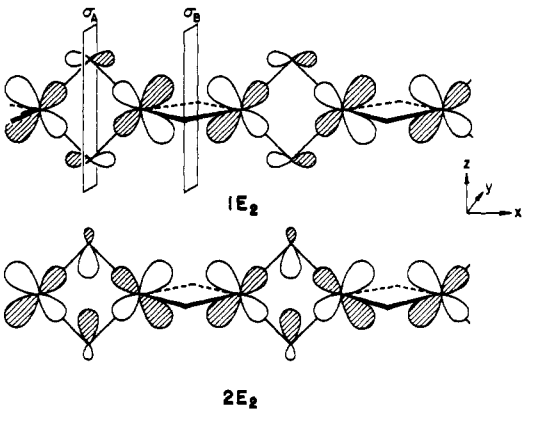

8

expect that the 2E orbitals would interact more strongly with the bridging ligands and would be pushed higher in energy than 1E; the splitting is actually 0.63 eV.

At X, the situation is a little different, as a result of the fact that all crystal orbitals with $k = \pi/a$ are antisymmetric with respect to a unit cell translation. All four crystal orbitals constructed from the dimer xz or xy orbitals will be antisymmetric with respect to either σ_A or σ_B. We can, however, identify two

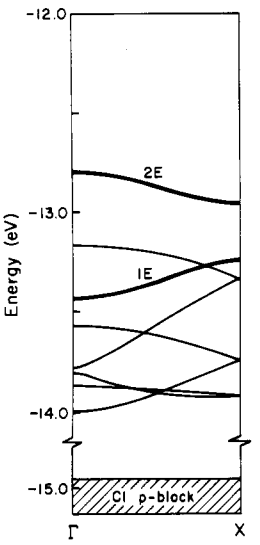

Figure 5. Band structure of the idealized (θ = 0°) chain.

distinct pairs of degenerate orbitals, as at Γ. One representative of each pair (the other being generated by the glide planes) is shown in **9**. $1E_2$ and $2E_2$, derived from xz_A and xz_B, respectively,

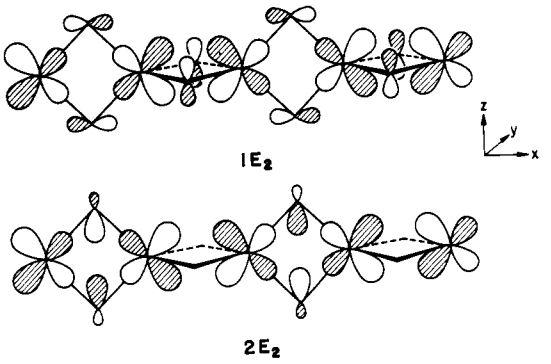

9

lie in the xz plane and as a result interact most strongly with the halide ligands in this plane, i.e. those that lie on σ_A. Since $2E_2$ is symmetric with respect to this plane and $1E_2$ antisymmetric, we can see that for this geometrical arrangement $2E_2$ will lie above $1E_2$. The overlaps with the ligands in the xy plane are larger for $1E_2$ than for $2E_2$ (where they are zero by symmetry), but these are weaker π-type overlaps and the effects of the ligands in the xz plane predominate. The 1E–2E splitting is, however, expected to be considerably smaller than it is at Γ. This can clearly be seen in the band structure of the undistorted chain **7**, which is shown in Figure 5. We have enough electrons in our mixed-valence systems to three-fourths fill the highest set of bands 2E. We will consider the question of how the electrons are distributed among the crystal orbitals after we have examined the effects on this band structure of the structural distortions of **1** and **3**.

Electronic Consequences of the Twist Distortions

As noted in the introduction, the observed structures **1** and **3** differ from our idealized model in having nonorthogonal X–Cu–X planes and in having a range of Cu–X distances. We have chosen to consider the consequences of these two individual components of the distortions separately, starting with the angular "twist" component.

Since it does not involve a change in the translational periodicity of the structure, the distortion of the bromide compound **3** will be considered first. For simplicity, and to allow comparison with our calculations on **1**, we have studied as a model a hypothetical chloride compound with the same interplanar angles. Geometrical details are given in the Appendix.

The distortion, as shown in **10**, involves the loss of the S_4 symmetry at the copper centers and the mirror planes σ_1 and σ_2 present in **7**. However, the glide planes g_1 and g_2 and the perpendicular mirror planes σ_A and σ_B are retained.

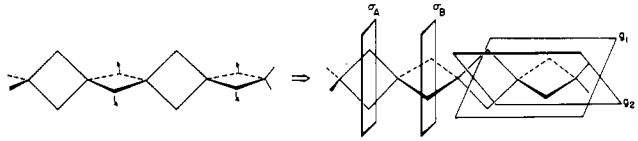

10

We can deduce some features of the new band structure from considerations of symmetry. The crystal wave functions at all points in the Brillouin zone must transform as one of the irreducible representations of the space group $\tilde{G}$. This is not the best place to describe the group-theoretical principles involved.[13a,b] We note, however, that the transformation properties under the pure translation operations of the space group can be labeled by the wave vector **k**. The transformation properties under the rotation operations of the space group are labeled by noting that each unique representation at a given **k** corresponds to a distinct representation of a much smaller group, which in this paper we will refer to rather loosely as $\tilde{G}_k$. Its size is the same as $\tilde{G}_k°$, the point group consisting of all operations in the point group of $\tilde{G}$ that transform **k** into itself or into another vector related to **k** by a primitive reciprocal lattice translation. For symmorphic space groups, and nonsymmorphic space groups when **k** terminates in the interior of the first Brillouin zone, $\tilde{G}_k$ is isomorphic with $\tilde{G}_k°$, and a symmetry classification quite analogous to the point group symmetry analysis in molecules can be used. At the zone edge, for a nonsymmorphic space group, this is not always the case, and dimensionalities and characters of the irreducible representations are best obtained from published tables.[13c]

We can simplify the description of these orbitals and learn something about the way their energies change with θ by returning to the local coordinate system described in **4** for the monomeric examples. We choose the y' and z' axes to be parallel to the 2-fold axes in the yz plane, as before. Since these 2-fold axes are contained in the planes g_1 and g_2, each of the four crystal orbitals under consideration can be written in terms of pure xy' or xz' contributions at each copper site. For θ = 0°, we have two degenerate pairs of orbitals. When discussed above, these were described in terms of their xy and xz components. We can reexpress the crystal orbitals in terms of the basis functions xy' and xz' by forming linear combinations. When this is done, it is found that one member of each E set is composed of xy' on every atom; the other is pure xz'. From this we can predict the first-order behavior of the orbital energies at Γ when distortion takes place. The crystal orbital composed of xz' will rise in energy, reflecting the behavior of this basis function as seen in Figure 1; the orbital composed of xy' will fall. These energy changes will initially be linear with θ.

At X we can reexpress the orbitals of **9** in a similar way. We find that each crystal orbital is composed of xy' on one of the copper atoms in the unit cell and xz' on the other. We can see that none of these crystal orbitals will experience a first-order change in energy on distortion, since the contributions on one copper are precisely canceled by those on the other. The consequent fact that the degeneracy at the zone edge is retained also follows from the translational symmetry. The presence of nonsymmorphic symmetry elements (g_1 and g_2) at all values of θ will ensure that all bands remain doubly degenerate at the zone edge.

The resulting bands are shown in Figure 6b, for θ = 5°. If we classify these bands according to the operations of $\tilde{G}_k$ (which here

(13) (a) Burns, G.; Glazer, A. M. *Space Groups for Solid State Scientists*; Academic Press: New York, 1978. (b) Cornwell, J. F. *Group Theory and Electronic Energy Bands in Solids*; Wiley: New York, 1969. (c) Kovalev, O. V. *Irreducible Representations of the Space Groups*; Gordon and Breach: New York, 1965.

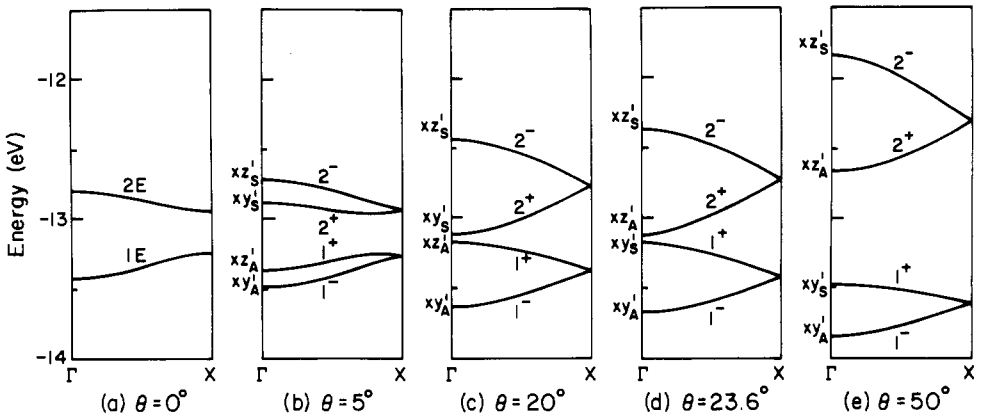

Figure 6. Schematic partial band structures for the twisted chain **10**, at various values of θ.

is isomorphic to C_{2v}), we find there are two distinct symmetries. They are labeled by superscript + and − in Figure 6, according to the character with respect to the glide plane g_1. At Γ, however, the four crystal orbitals are symmetry distrinct and are labeled according to their composition (xy' or xz') and symmetry with respect to the plane σ_A.

As θ increases, mixing between bands 1^+ and 2^+, and to a lesser extent between 1^- and 2^-, will increase in the interior and at the edge of the zone, but the higher symmetry at Γ ensures that xy'_S and xz'_A do not mix, as they become closer in energy. At a particular value of θ xy'_S will have a lower energy than xz'_A, but since bands 1^+ and 2^+ cannot cross, the correlation, or connectivity, of the bands must change at this point, as shown in Figure 6c,d. Further distortion will then increase the splitting between bands 1^+ and 2^+, as shown in Figure 6e. Another consequence of the mixing between 1^+ and 2^+ is that the "center of gravity" of the pair of bands 2^+, 2^- will rise, mainly because of the mixing of xz' character into 2^+, and that of 1^-, 1^+ will fall. For our band occupation of nine electrons we are therefore able to identify both first- and second-order stabilizing contributions to the total energy on distortion. The first-order effect arises from the splitting of the 2E levels as one goes from part a to part b of Figure 6. This effect is clearly a solid-state analogue of the first-order Jahn–Teller distortion which favors the twisting in $CuCl_4^{2-}$. In moving from the dimer to the polymer, we have regained some of the symmetry we lost when two monomers were coupled together, and so we have also regained a first-order contribution to the energy change. The mixing between the bands in the Brillouin zone provides the second-order effect.

We can obtain an estimate of the energy gained as a result of distortion by calculating the sum of one-electron energies at a number of values of θ. When this is done, assuming a single occupation of all of the crystal orbitals of the 2^- band (vide infra), we find a maximum stabilization at $\theta \approx 15°$ of around 0.09 eV. The curve is very similar to the $d^{9.5}$ curve in Figure 2, highlighting the relationship between the infinite material and a rather weakly coupled arrangement of dimers.

In Figure 7 we have plotted the Cu d part of the band structure for the observed value of $\theta = 23.6°$. The pertinent orbitals are labeled as in Figure 6. The total density of states (DOS) is shown at the far right, together with the projected contributions to this DOS from the copper xy' and xz' orbitals. These projections show the effect of mixing between orbitals 1^+ and 2^+. At $\theta = 0°$ these orbitals are pure xz' and xy', respectively, and in Figure 7 these compositions have been interchanged, showing the importance of the ligand field splitting. The dispersion of the bands is a direct result of the through-ligand coupling interactions, since it can be measured by the energy difference between the xz'_A and xz'_S and the xy'_A and zy'_S crystal orbitals at Γ.

So far, the twisting distortion we have examined has retained the equivalence of the two copper atoms. **3** has inequivalent copper sites; the Cu–Br bond lengths are shorter for one copper than the other. This distortion clearly lowers the symmetry of the chain

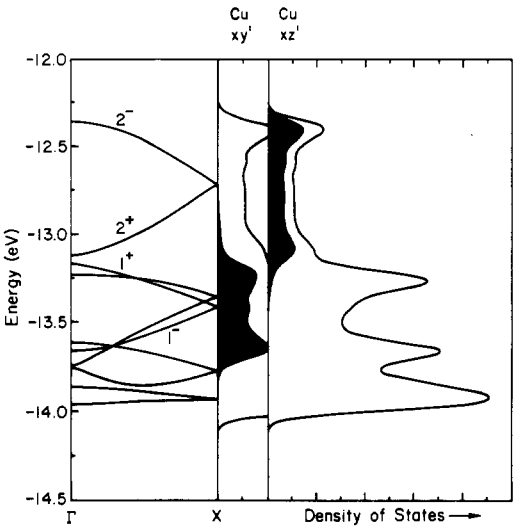

Figure 7. Band structure of **10** with $\theta = 23.6°$. Total DOS and the contribution to this DOS from the Cu xy' and xz' orbitals are shown.

further, removing σ_A, σ_B, and the glide planes g_1 and g_2 of **10**. This distortion is shown schematically in **11** and the resultant

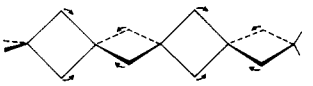

11

change in band structure for our $[CuCl_2]_\infty$ model in **12**. The

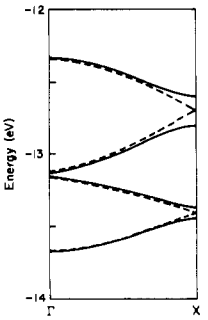

12

bands corresponding to the structure with equal Cu–Cl bond lengths are shown by dotted lines. The main result is as expected from considerations of symmetry—the loss of the 2-fold degeneracy of all bands at X. There is an obvious similarity here with the Peierls distortion; here it is the halide ligands that are undergoing

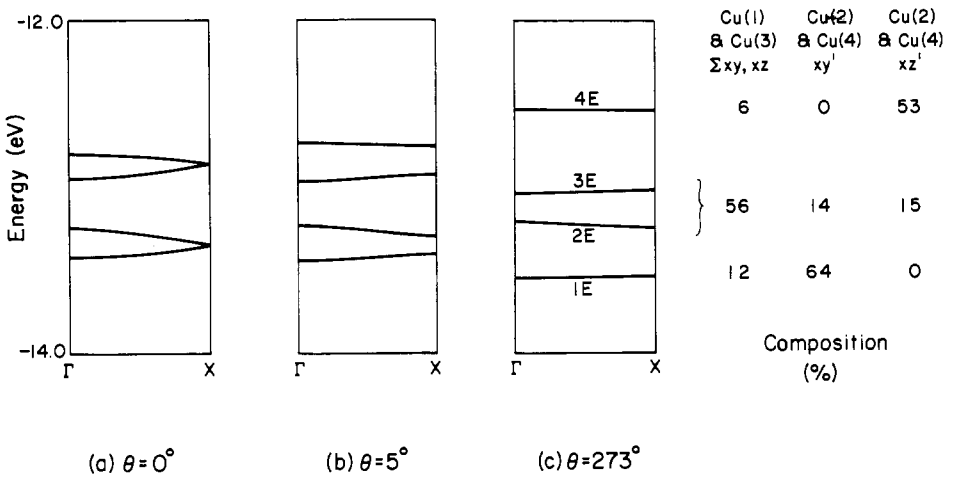

Figure 8. Schematic partial band structures for the twisted chain **13**, for selected values of θ. For $\theta = 27.3°$ the percentage compositions in terms of the relevant copper orbitals are shown.

the "pairing" rather than the copper atoms.

Before we consider the electronic consequences of the distortion observed in **1**, which has a unit cell containing four $CuCl_2$ units, we must consider the appearance of the band structure of our ideal structure **7** when the unit cell is redefined. The doubling of the unit cell will halve the size of the reciprocal cell, the Brillouin zone, and will double the number of bands. This process is conceptually most easily achieved by "folding" the band structure of Figure 5 about $k = \pi/2a$. The result is shown to the left of Figure 8. As before, we will focus first on the angular part of the distortion and then consider the consequences of the changes in bond length.

The distortion is shown schematically in **13**. S_4 site symmetry

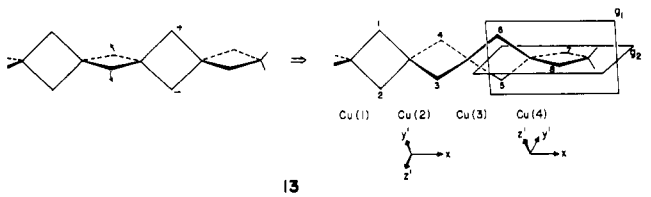

13

is retained at Cu(1) and Cu(3), while the twisting distortion imposes D_2 symmetry at Cu(2) and Cu(4). As before, we will use local coordinate systems at Cu(2) and Cu(4) to describe the crystal orbitals when ligand field splitting effects become important. Since the twists at Cu(2) and Cu(4) are in opposite directions, the y' and z' axes defined at these centers will not be parallel but will be rotated 90° relative to each other, as shown in **13**. We have also shown in **13** the two orthogonal glide planes g_1 and g_2. g_1 relates ligand sites 1 and 6; g_2 relates sites 3 and 8. As $\theta \rightarrow 0°$, these planes become coplanar with σ_1 and σ_2 of **7**.

As before, we can consider the effect of symmetry and orbital composition on the way the band structures change when $\theta > 0°$. At the Γ point the group of **k** is isomorphic with D_{2d} and so crystal orbitals that are antisymmetric with respect to the C_{2x} axis should remain doubly degenerate. At X, the presence of the glide planes ensures that all crystal orbitals will be doubly degenerate, but the quadruple degeneracies that resulted from the folding back of doubly degenerate levels, and were therefore the direct result of the higher translational symmetry of the undistorted structure, are lost. In the interior of the zone the group of **k** contains only four symmetry operations (E, C_{2x}, g_1, g_2) and thus has order 4. Therefore, either there are four 1D representations or there is one 2D representation. The band structure shows the presence of both singly and doubly degenerate crystal orbitals—which seems at first inconsistent with both of these alternatives. There are in fact four 1D representations (the group is isomorphic to C_{2v} at this point), and the extra degeneracies are the result of time-reversal symmetry.[13b]

The simplest way to deduce the first-order energy changes on distortion is to reexpress the crystal orbitals in terms of their compositions on Cu(2) and Cu(4). Only these centers are actually undergoing the twist distortion, and we can ignore Cu(2) and Cu(3) in our examination of the first-order effects. At Γ, and $\theta = 0°$, the relationship between a given crystal orbital's composition at Cu(2) and that at Cu(4) can be deduced from the fact that before we redefined the unit cell these atoms were related by a primitive translation. Therefore, the crystal orbitals at the Γ point (of the larger unit cell) will be either symmetric or antisymmetric with respect to this translation. In both cases the orbital compositions at Cu(2) and Cu(4) will be the same. When reexpressing these orbitals in terms of the "local" basis, we must recall that the local coordinate systems on these two centers are rotated by 90° relative to each other. If a crystal orbital has a contribution from xy' on Cu(2), it will therefore have an equal contribution from xy' on Cu(4). From this we can see that there will be no first-order energy change to these crystal orbitals on distortion. By contrast, at X in the new Brillouin zone the crystal orbitals all originated from the point $\pi/2a$ in our original choice of Brillouin zone. These orbitals have a change of phase every two cells (every four copper atoms); their nodes and maxima are spaced by two copper sites relative to each other. This suggests that if we can choose suitable linear combinations we can form from each of the quadruply degenerate sets of orbitals at X in Figure 8a four orbitals with the following compositions Cu(2) and Cu(4): (i) Cu(2) xz'; (ii) Cu(4) xz'; (iii) Cu(2) xy'; (iv) Cu(4) xy'. Clearly on distortion (i) and (ii) will rise in energy and remain degenerate; likewise (iii) and (iv) will fall, a result consistent with the group-theoretical considerations. We should note here that although for our partially occupied system of bands this loss of degeneracy at the zone boundary should be stabilizing, the small dispersion of bands 1E and 2E in Figure 5 will mean that the actual energies involved here will be very small. The results of these first-order changes are clearly shown in Figure 8b, calculated with $\theta = 5°$. (For clarity we have only included those bands derived from xz and xy orbitals on the copper atoms.)

Just as in the case of the first distortion, there are second-order effets to consider as well. Mixing between the four E sets will take place. The overall result resembles closely the behavior of the orbitals of the $Cu_2Cl_6^{3-}$ dimer from Figure 4, when one center is subjected to the twist distortion. At $\theta = 0°$ the composition of the orbitals reflects the nature of the coupling via the bridging ligands—as θ increases, the composition of the orbitals will start to reflect the ligand field effects. The highest degenerate pair (4E in Figure 8) will mix in more xz' character on Cu(2) and Cu(4), throughout the Brillouin zone. The lowest E set will also be localized on these atoms, but xy' character will predominate. The two remaining orbitals will localize on Cu(2) and Cu(3). The extent to which this has happened, at $\theta = 27.3°$, is indicated by the percentage compositions given next to Figure 8c. The fact that these do not sum to 100 reflects the fact that there is some mixing of these d orbitals into the Cl p block and some Cl

character in the orbitals 1E–4E.

Since the highest orbitals 4E are only half-occupied, their localization on Cu(2) and Cu(4) will make these atoms more positively charged than Cu(1) and Cu(3). A rough estimate of this effect is provided by the Mulliken atomic populations, +0.22 on Cu(1) and Cu(3) and +0.64 on Cu(2) and Cu(4).

Clearly, we can identify Cu(2) and Cu(4) as the formal Cu(II) atoms in this mixed-valence compound. The second stage of the distortion, the inequivalence of bond lengths, is entirely consistent with this charge localization. In contrast to the distortion **11**, the symmetry of the chain is unaffected and the only changes that result in the band structure (Figure 8c) are a slight rise in energy of 4E and a lowering of 1E. This reflects an increase in the strength of ligand field splitting at the Cu(II) centers.

In our calculations, the total energy reaches a minimum at around $\theta = 20°$, somewhat lower than the observed value. The minimum is rather shallow and corresponds to an energy 0.13 eV per Cu(I)–Cu(II) unit lower than that of the undistorted geometry.

Band Filling and Physical Properties

Much of the interest in one-dimensional materials stems from the variety of physical properties they exhibit.[14] In many important cases, these properties are the macroscopic manifestations of electronic instabilities that arise from the presence of partially filled bands. The consequences of the partially filled band depend crucially on the distribution of th e electrons among the available crystal orbitals. One-electron band theory would predict that in the ground state the lowest energy crystal orbitals would be doubly occupied by spin-paired electrons, giving rise to nonmagnetic, metallic properties. However, as a result of interelectronic interactions, other orbital occupations, giving rise to magnetic states, and also charge and spin density waves may result. The reader is referred to the work of Whangbo[2c,15] for a discussion of the factors that affect the relative stabilities of these states.

It is obviously difficult, within the framework of our one-electron calculations, to make predictions about physical properties that depend critically on the orbital occupation in the ground state. Very little physical data are available for **1** and **3** at present. However, it is worth considering some of the possible orbital occupation schemes that might reasonably be adopted and the physical properties that might result from them.

We will consider first the band structure of the idealized structure **7**, as shown in Figure 5. The highest band in the d block, 2E, is shown in **14**. The filling representation shown to the right

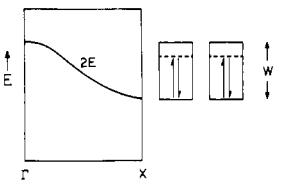

14

is that for a metallic state. Each box represents one component of the E set, and both are three-fourths filled with spin-paired electrons. In **15** we show two alternative schemes. Both **15a** and

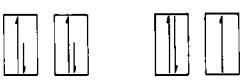

15a **15b**

15b are magnetic states and from Whangbo's analysis[9c,15] are expected to be lower in energy than **14** when the band width (W in **14**) is small compared with the "on-site" Coulombic repulsion integral, U. U is defined by reexpressing the delocalized crystal orbitals in terms of orthogonal localized basis functions. U is then the Coulombic interaction integral between two electrons in the same localized orbital. Few estimates of U exist, and they span a wide range of values, from less than 1 eV to more than 10 eV.[2c,9c,15] However, it seems likely that for an electronegative metal such as copper, with relatively contracted d orbitals, the on-site repulsion integrals will be quite large compared to those of other first-row transition elements, and U values in excess of 1 or 2 eV are quite possible. We might expect for this hypothetical, ideal structure with a band width $W = 0.15$ eV that a magnetic insulating state would probably be formed. By similar arguments,[15b] Whangbo has shown that when $W > \sim 0.6U$ the state **15b** will be favored over **15a**.

It should be noted here that the representation **15b**, in which all the unpaired electrons are shown to have the same spin, does not necessarily imply that the material will show strong ferromagnetic coupling. When W is small, a description in which the unpaired electrons are quite localized on different sites is usually applicable, and the ferromagnetic contribution to the observed magnetic exchange coupling will depend on the precise nature of the interaction between the localized magnetic orbitals. However, a narrow bandwidth does tend to reduce the antiferromagnetic contribution to the exchange coupling, since the contribution of nonmagnetic states such as **14** becomes less important. A quantitative relationship between bandwidth and antiferromagnetic coupling has been suggested by Kahn et al.;[16] using their expression within the Wolfsberg–Helmholtz approximation[17] indicates that a bandwidth of 0.15 eV in the $[CuCl_2]_\infty$ chain should contribute about -5 cm^{-1} to the coupling constant J.

It is interesting to consider the types of structural distortions that might be expected to arise from the band fillings **14**, **15a**, and **15b**. The distortion expected for a three-fourths-filled band, as for a one-fourth-filled band, is a tetramerization—a distortion that would create a band gap at the Fermi level of **14** by quadrupling the unit cell to eight copper atoms. The fact that this distortion is not observed is consistent with our expectations that this structure would probably have a magnetic insulating ground state. **15a** might be predicted to undergo the same types of distortions as a half-filled band. A dimerization distortion would lead to the orbital filling scheme shown in **16**. Clearly, the

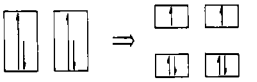

16

$[CuCl_2^-]_\infty$ distortion **13** is an example of this type. The distortion removes the metallic character, and we might expect **1** to be a magnetic insulator. The highest degenerate pair of orbitals are localized on the Cu(II) atoms, and the very narrow bandwidth (<0.001 eV) reflects the fact that there is very little interaction between these centers. This is reasonable since the Cu(II) centers are separated by 6.2 Å. It is probably appropriate to regard the unpaired electrons as residing in localized magnetic orbitals on the Cu(II) centers; rather little magnetic exchange coupling is expected in this system. Even if it were possible to partially oxidize this chain, the extremely narrow bandwidth would probably preclude any appreciable electrical conductivity.

In contrast, the state of occupation **15b** would not be expected to lead to a pairing distortion. Instead, it is stabilized by a distortion that removes the degeneracy between the two 2E orbitals. This is achieved by the twisting distortion **10**. The evolution of the band structure shown in Figure 6 is summarized in **17a–c**. **17d** shows the result of the bond-length distortion (**11**) that breaks the degeneracy of these two bands at X. Once again we would

(14) See for example ref 1a.
(15) (a) Whangbo, M.-H. *J. Chem. Phys.* **1980**, *73*, 3854; **1981**, *75*, 4983; *Acc. Chem. Res.* **1983**, *16*, 95. (b) Whangbo, M.-H. *Inorg. Chem.* **1980**, *19*, 1728. (c) Whangbo, M.-H. In *Extended Linear Chain Compounds*; Miller, J. S., Ed.; Plenum: New York, 1982; Vol. 2.
(16) (a) Girerd, J.-J.; Charlot, M.-F.; Kahn, O. *Mol. Phys.* **1977**, *34*, 1063. (b) Charlot, M.-F.; Girerd, J.-J.; Kahn, O. *Phys. Status Solidi* **1978**, *B86*, 497. (c) See also ref 2c and 12.
(17) Hoffmann, R. *J. Chem. Phys.* **1963**, *39*, 1397. Hoffmann, R.; Lipscomb, W. N. *J. Chem. Phys.* **1962**, *36*, 2179.

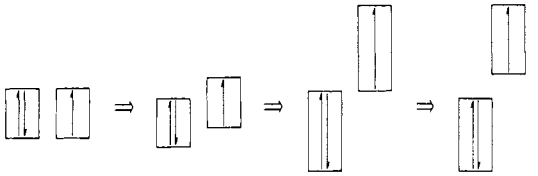

17a 17b 17c 17d

expect a magnetic insulating state. Here $W \approx 3$ eV for the singly occupied band, and we might anticipate slightly stronger antiferromagnetic coupling; use of the expression of Kahn et al. gives an estimate for the antiferromagnetic contribution to the exchange coupling of ~ -20 cm^{-1}.

Conclusions

In this paper we have presented calculated band structures for the two newly characterized compounds **1** and **3**, with an emphasis on the way these band structures are related to simpler systems. The prototype complex is a $CuCl_4^{2-}$ ion of S_4 symmetry, which is stabilized by a Jahn–Teller distortion that breaks the orbital degeneracy. When these centers are coupled together to form a polymeric material, the principal interactions between the copper centers arise through the bridging ligands. The twisting distortion observed in **3** breaks the S_4 symmetry of the polymer and thus removes a degeneracy at all points of the Brillouin zone, except the zone edge. This last degeneracy is lost by a "pairing" distortion of the ligands, which helps to stabilize a localized mixed-valence state. The alternative lowering of symmetry observed in **1** does not break the S_4 symmetry and does not have such strong first-order character. In the behavior of the orbitals, this system, with a unit cell of four copper atoms, closely resembles a coupled assembly of mixed-valence dimers. They are undergoing a cooperative distortion in which one copper center in each dimer is twisted to D_2 symmetry.

The calculated stabilizations for these effects are quite small, and we anticipate the conformational surface of these polymers to be soft. It is likely that crystal-packing forces play an important role in determining the solid-state structures of materials of this type.

We hope that our work will aid the understanding of the physical properties of these materials. The narrow bandwidths obtained in our calculations suggest that the ground state will be a magnetic insulating one and that, especially in the case of the chloride compound, a description in terms of localized magnetic orbitals should be useful. The exact nature of the magnetic coupling is difficult to predict from our calculational approach, but we do not expect it to be very large.

Acknowledgment. We are grateful to Roger Willett for providing the inspiration for this study, as well as some data prior to publication. P.S.'s stay at Cornell was made possible by a stipend from the University of Bristol, and we thank Prof. F. G. A. Stone for arranging this stay. P.S. is grateful to the members of our research group for their advice and counsel, especially Jing Li and Marja Zonnevylle. We thank Joyce Barrows for the typing and Jane Jorgensen and Elisabeth Fields for the drawings. Our work was supported by the National Science Foundation through Research Grant CHE8406119.

Appendix

All computations were carried out by using the extended Hückel method;[17] those on one-dimensional materials used a tight-binding scheme.[18] The basis set parameters were taken from previous work (H_{ii} followed by STO exponent): Cu[19] 4s, −11.40 eV, 2.20; Cu 4p, −6.06 eV, 2.20; Cu 3d, −14.00 eV, 5.95 (0.5933), 2.30 (0.5744) (a double-ζ expansion was used, the expansion coefficients are given in parentheses); Cl[20] 3s, −30.0 eV, 2.033; Cl 3p, −15.0 eV, 2.033. Properties were averaged over the Brillouin zone by using a 20-k-point set.

The geometries used in the calculations were taken from **1**.[4] The bromide compound **3** was modeled by a chloride compound with bond lengths taken from **1** and appropriate interplanar angles from **3**. These calculations in which all Cu–Cl bond lengths were set equal had Cu–Cl = 2.30 Å and Cu–Cu = 3.10 Å. The remainder had Cu^{I}–Cl = 2.34 Å and Cu^{II}–Cl = 2.25 Å.

(18) Whangbo, M.-H.; Hoffmann, R.; Woodward, R. B. *Proc. R. Soc. London, Ser. A* **1979**, *366*, 23.
(19) The H_{ii} values were taken from ref 12 and the Slater exponents from ref 11.
(20) Anderson, A. B.; Hoffmann, R. *J. Chem. Phys.* **1974**, *60*, 4271.